Structure of Habit-Modifying Trivalent Transition Metal Cations (Mn^{3+}, Cr^{3+}) in Nearly Perfect Single Crystals of Potassium Dihydrogen Phosphate As Examined by X-ray Standing Waves, X-ray Absorption Spectroscopy, and Molecular Modeling

Xiaojun Lai* and Kevin J. Roberts

Institute of Particle Science and Engineering, School of Process, Environmental and Materials Engineering, University of Leeds, Leeds LS2 9JT, United Kingdom

Michael J. Bedzyk and Paul F. Lyman

Department of Materials Science and Engineering, Northwestern University, Evanston, Illinois 60208

Lisandro P. Cardoso

IFGW, Universidade Estadual de Campinas (UNICAMP, CP6165, 13083−970), Campinas, SP, Brazil

José M. Sasaki

Dep. Fisica, Universidade Federal do Ceará, 60455−760, Fortaleza, Ce, Brazil

Received December 5, 2004. Revised Manuscript Received May 9, 2005

The local atomic structure of habit-modifying transition metal cations within the crystal lattice of potassium dihydrogen phosphate (KDP) is investigated using X-ray absorption spectroscopy (XAS) and X-ray standing wave (XSW) spectroscopy, together with molecular modeling. XAS reveals the transition metal cations to be structurally incorporated into the crystal lattice as an ionic complex that is octahedrally coordinated to two phosphate groups and four water molecules. The position of transition metal cation, as determined by XSW, is consistent with its location at an interstitial lattice site, with a coherent position 0.66 with respect to the {200} crystal lattice planes. The structural model suggested that the transition metal complex mimics the surface structure of KDP prismatic {100} face, hence facilitating its adsorption on this face. Charge compensation associated with the impurity incorporation during crystal growth is effected via the hydrated impurity complex displacing one bonding proton that binds two phosphate groups together with two potassium ions within the crystal structure to maintain the system charge balance. The resulting model is consistent with the XAS and XSW results as well as earlier work (Barrett, N.; Lamble, G. M.; Roberts, K. J.; Sherwood, J. N.; Greaves, G. N.; Davey, R. J.; Oldman, R. J.; Jones, D. *J. Cryst. Growth* **1989**, *94*, 689), albeit contrasting with our preliminary data on the isomorphous ammonium dihydrogen phosphate in which a substitutional model was proposed (Cunningham, D. A. H.; Hammond, R. B.; Lai, X.; Roberts, K. J. *Chem. Mater.* **1995**, *7* (9), 1690).

1. Introduction

The optimization of crystal shape and size is important in industrial crystallization,[3] as crystal morphology and size have an impact on a number of important technological areas, including downstream production processes such as filterability, storage, and compaction. In this, poorly defined crystal habits can often be due to undesired impurities being present during crystallization. Conversely, habit-modifying additives are often used to optimize crystal morphology through their ability to preferentially bind to specific crystal faces and hence change their relative growth rates. Such heterogeneous species are presumed to affect the growth of individual crystal faces, either by blocking the movement of the growth step or by incorporating in the solid-state and disrupting the intermolecular bonding networks within the crystal structure. However, due to their effective action at quite low concentration, detailed structural studies of local atomic chemistry of habit-modifying species within the crystal lattice can be very challenging. Thus, only few habit modification systems have been fully characterized, and as a result, much concerning the physical and mechanistic processes associated with their molecular-scale action remains unknown.

Potassium and ammonium dihydrogen phosphate (KDP and ADP) have been studied extensively because of the importance of their wide range of applications as ferroelectric and electrooptic materials, especially reflecting the demand for large, perfect, single crystals for advanced laser technology applications.[4] In addition, this system has often been used as a representative model system for defining the physical mechanisms that underpin particle formation processes in industrial crystallization due to its comparative ease of growth and high growth and high crystal perfection. KDP

* To whom correspondence should be addressed. E-mail: chexl@leeds.ac.uk.

(1) Barrett, N.; Lamble, G. M.; Roberts, K. J.; Sherwood, J. N.; Greaves, G. N.; Davey, R. J.; Oldman, R. J.; Jones, D. *J. Cryst. Growth* **1989**, *94*, 689.
(2) Cunningham, D. A. H.; Hammond, R. B.; Lai, X.; Roberts, K. J. *Chem. Mater.* **1995**, *7* (9), 1690.
(3) Kolb, H.; Comer, J. J. *J. Am. Chem. Soc.* **1945**, *67*, 894.
(4) De Yoreo, J. J.; Burnham, A. K.; Whitman, P. K. *Int. Mater. Rev.* **2002**, *47* (3), 113−152.

10.1021/cm0478881 CCC: $30.25
Published on Web 07/07/2005

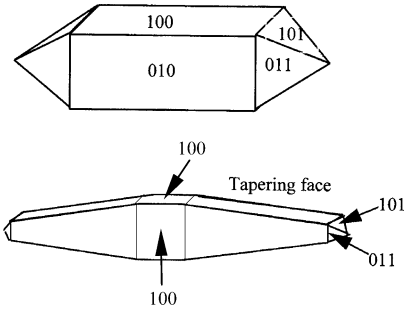

Figure 1. Schematic presentation showing the typical growth morphologies for KDP crystals: (top) pure KDP and (bottom) impurity-doped KDP.

and ADP are also well-known demonstration systems for the study of the effects of habit modification by ionic species.[5−11] In the presence of trace amounts of trivalent transition metal cations, KDP and ADP crystals become elongated along the *c*-axis associated with these impurities, being preferentially incorporated into the prismatic (100) and (010) crystal growth sectors. This incorporation results in these faces becoming tapered (see Figure 1). In particular, there is a surprising lack of understanding of both the local and long-range (crystallographic) structural nature of the modifying impurities together with their bonding environment within the host crystal lattice.

Several studies have provided structural models for the impurity species as incorporated within the crystal lattice. Electron nuclear double resonance (ENDOR) studies[12,13] have suggested that the Cr^{3+} substitutes for one K^+ and two H^+ vacancies at an interstitial site when incorporated into the crystal. Drawing upon Mössbauer spectroscopy studies,[10,14] Barrett[1] used glancing angle XAS to study Fe^{3+}-doped ADP crystals and proposed that Fe^{3+} ions are coordinated with two oxygen and two phosphorus atoms through an interstitial model with Fe^{3+} ion located at the (0.22, 0.25, 0.125) lattice site. In this model, the Fe^{3+} was proposed to be incorporated in the crystal lattice as a bare ion disturbing the hydrogen-bonding network in the lattice and setting up new bonds between two phosphate groups through the bridging oxygens (see Figure 2). However, in this work, the mechanism of either charge compensation or ionic desolvation from the solution state was not defined.

Cunningham et al.[2] studied Cr^{3+}-doped ADP crystals by applying XAS and UV−vis spectroscopy to examine the nature of the incorporated ionic species. This work contrasted with the earlier work of Barrett et al.,[1] in that an interstitial incorporation model was proposed. In this, a single phosphate ion was proposed to be replaced by a $CrCl_2(H_2O)_4^+$ complex with formal charge compensation being achieved through the removal of two hydrogen-bonding protons from adjacent phosphate groups or two adjacent ammonium cations (Figure 3). However, direct validation of this tentative model via detailed structural studies was not carried out.

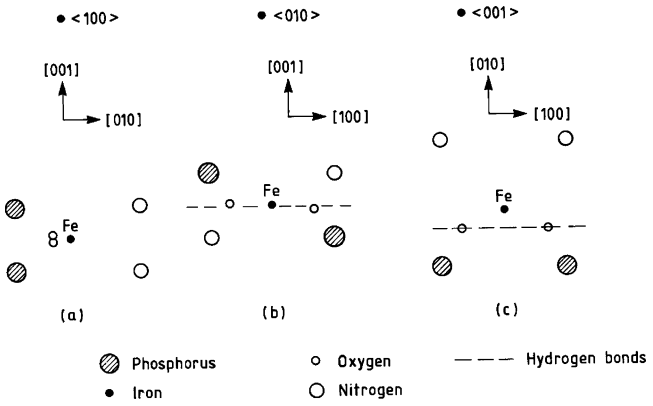

Figure 2. Barrett et al.[1] suggested that Fe incorporated in ADP crystal occupies an interstitial site (0.25, 0.22, 0.125) seen along the three crystallographic axes: (a) [100]; (b) [010]; (c) [001].

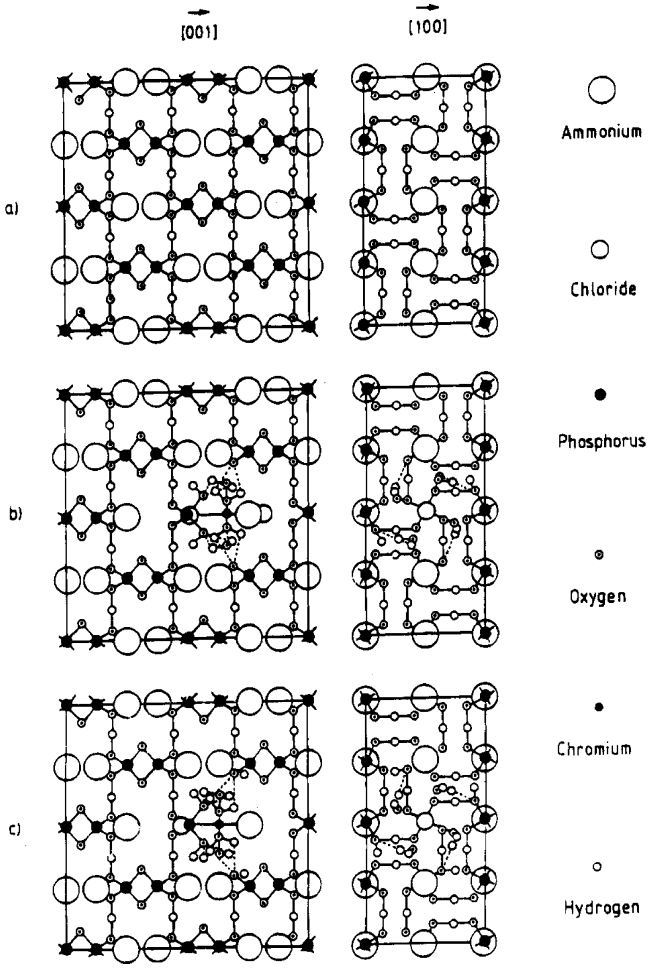

Figure 3. Pure and $CrCl_2(H_2O)_4^+$-doped ADP crystal lattice projection in the Cunningham structure model.[2] The left and right columns of the figure present the projections of the ADP crystal lattice down the *a*-axis and *c*-axis, respectively. (a) pure ADP crystal lattice; (b) ADP crystal lattice with $CrCl_2(H_2O)_4^+$-impurity complex occupying a phosphate site with removal of two hydrogen-bonding protons from adjacent phosphate groups; (c) ADP crystal lattice with $CrCl_2(H_2O)_4^+$ impurity complex occupying a phosphate site with removal of two adjacent ammonium groups.

(5) Jaffe, H.; Kjellgren, B. R. F. *Faraday Discuss., Cryst. Growth* **1951**, *5*, 319.
(6) Mullin, J. W.; Amatavivadhana, A.; Chakraborty, M. *J. Appl. Chem.* **1970**, *20*, 153.
(7) Davey, R. J.; Mullin, J. W. *J. Cryst. Growth* **1974**, *23*, 89.
(8) Davey, R. J.; Mullin, J. W. *J. Cryst. Growth* **1974**, *26*, 45.
(9) Davey, R. J.; Mullin, J. W. *Kristall. Techn.* **1976**, *11* (3), 229.
(10) Fontcuberta, J.; Rofriguez, R.; Teheda, J. *J. Cryst. Growth* **1978**, *44*, 593.
(11) Mullin, J. W. *Crystallization*, 3rd ed.; Butterworth-Heinemann: Woburn, MA, 1992.
(12) Bravo, D.; Lopez, F. J.; Dieguez, E.; Aguilar, M.; Cabrera, J. M. *J. Phys.: Condensed Matter* **1989**, *1*, 6145.
(13) Bravo, D.; Bottcher, R.; Lopez, F. J. *J. Phys.: Condensed Matter* **1992**, *4*, 2297.
(14) Wang, W.; Chao, Y.; Zhang, Y.; Wang, Z. *Chin. Phys. Lett.* **1987**, *4*, 333.

More recently, Lai et al.[15] used X-ray multiple diffraction to study Mn^{3+}-doped KDP. This work confirmed this species to be chemically bonded within the crystal lattice, consistent with incorporation at an interstitial rather than at a substitutional lattice site.

de Vries et al.[16] used X-ray scattering to examine the surface atomic structure of the habit faces of KDP. Their study revealed that the positively charged {101} face, which contains only K^+, would provide a large barrier to adsorption of a positively charged metal ion impurity. In contrast, the prismatic {100} face contains both K^+ and $H_2PO_4^-$ at the growth interface, hence enabling more readily cationic impurity adsorption onto this surface.

Drawing the above together, the purpose of this paper is to report on further work aiming to resolve the atomic scale nature of this impurity incorporation site. In this, the structural environment of the impurity complex within the crystal lattice has been investigated by using XAS and XSW combined with molecular modeling. Here, XAS is used to examine the local atomic coordination around the cationic impurity, the XSW technique is used to determine the location of the impurity with respect to the underlying crystal lattice, and molecular modeling is used to build up a structural model for the impurity incorporated within the crystal lattice.

2. Experimental Section

2.1. Crystal Growth. Nearly perfect single crystals of KDP were grown from seeded aqueous solutions by lowering the solution temperature at the cooling rate of 0.5°/day. $CrCl_3$ was added to the KDP solution to prepare Cr^{3+}-doped samples. Mn^{3+}-doped samples were prepared by adding $KMnO_4$ and $MnCl_2$ at a 1:1 molar ratio[17] to the growth solutions. The Cr-doped crystals were grown at different pH solutions from pH 3.8 to pH 7, while the Mn^{3+}-doped crystals were grown from pH 1.5 to pH 3.5 solutions.

2.2. X-ray Absorption Spectroscopy. X-ray absorption spectra at the Cr K-edge (5889 eV) and Mn K-edge (6539 eV) were taken for the model compounds and for Cr- and Mn-doped single crystals of KDP using stations 8.1 and 9.3 at the Daresbury Synchrotron Radiation Source (SRS). The model compounds for Cr^{3+}-doped KDP were Cr foil and $CrPO_4$, and the model compounds for Mn^{3+}-doped KDP were Mn foil, $MnCl_2$, manganic acelylacetonate, K_2MnO_3, and $KMnO_4$. The model compounds were made into pellets using polystyrene as binding agent and diluent with the spectra being collected in transmission mode using ion chambers (e.g. see Figure 4a). The spectra for the single-crystal samples were taken in fluorescence mode using a Canberra 13-element Ge solid-state detector. To obtain the orientation information of the impurity species in the crystal lattice, single crystals of Cr- and Mn-doped KDP were aligned in the beam with a particular angle between crystal *c*-axis and the polarization direction of the X-ray beam, i.e., 15°, 45°, and 75°, respectively (see Figure 4b). From the absorption spectra, the extended absorption fine structure (EXAFS) was extracted to obtain the structural information in terms of the radial arrangement of the atoms around the absorption central atom. The data analysis employed XAS deduction and fitting of the EXAFS data using standard analysis techniques and software (EXCALIB, EXBACK, and EXCURV92). Full details of the experimental arrangement and associated data analysis are described in refs 18 and 19.

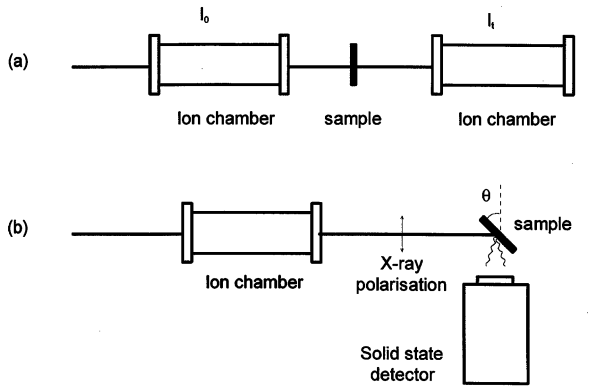

Figure 4. Schematic illustration of the experimental setup for X-ray absorption spectroscopy using stations 8.1 and 9.3 at the SRS, Daresbury. (a) Experimental setup in transmission mode to collect spectra of model compounds (b) Experimental setup in fluorescence mode to collect spectra of Cr^{3+}- and Mn^{3+}-doped single-crystal samples with varying beam incidence angles.

2.3. X-ray Standing Wave Spectroscopy. When a nearly perfect single crystal is placed in an X-ray beam, diffraction will only occur at certain (Bragg) angles, which are defined by the lattice parameters of the crystal. On diffraction of the X-rays, a standing wave is generated when dynamical X-ray interference occurs between incident and reflected beams (e.g. see Figure 5a). As the angle of incidence between the X-ray beam and the crystal surface changes, the nodes of XSW shift from a position located between atomic layers of the crystal (inset A of Figure 5b) to one where they are located directly on the lattice atomic layers (e.g. see inset B of Figure 5b). The latter case results in X-ray absorption and an associated enhancement of the X-ray fluorescence for the elements of the host crystal material, hence giving rise to an intensity reduction on the rocking curve. Thus, in the XSW technique, by controlling the incident angle of the X-ray beam, the position of the nodal planes of XSW can be controlled and coupled with simultaneous measurement of the fluorescence generated from an atom that is stimulated by X-ray at the standing wave node. Therefore, the positions of the atoms in the crystal, with respect to the atomic reflecting planes, can in principle be measured through the position of fluorescence yield relative to the rocking curve. Providing that the atomic species of the impurity is different from that of the host, the atomic X-ray fluorescence signal of the impurity can be easily distinguished from that of the host material species, with the fluorescence as a function of diffraction angle being used to determine the coherent position of the impurity atom with respect to the crystal lattice planes.

The impurity atom position relative the crystal lattice planes can be accurately calculated using the dynamic theory of X-ray diffraction[20,21] according to the fluorescence yield (Y_{sc}^{H}) given by

$$Y_{sc}^{H} = 1 + R + 2\sqrt{R}F^{H}\cos(\upsilon - 2\pi P^{H}) \qquad (1)$$

where $\sqrt{R}$ relates the amplitude of the diffracted beam (E_H) to that

(15) Lai, X.; Roberts, K. J.; Avanci, L. H.; Cardoso, L. P.; Sasaki, J. M. *J. Appl. Crystallogr.* **2003**, *36*, 1230.
(16) de Vries, S. A.; Goedtkindt, P.; Huisman, W. J.; et al. *J. Cryst. Growth* **1999**, *205* (1−2), 202.
(17) Zizic, B.; Davey, R. J.; Zegarac, T.; Pastor, T.; Ristic, R.; Napijalo, M. M. *J. Cryst. Growth* **1980**, *49*, 675.
(18) Armstrong, D. R.; Cunningham, D. A. H.; Roberts, K. J.; Sherwood, J. N. *X-ray Absorption Fine Structure*; Hasnain, S., Ed.; Ellis Horwood: Chichester, 1991; p 435.
(19) Lai, X. The Molecular Scale Mechanism Involved in the Habit Modification of KDP by Transition Metal Cations (Ph.D. Thesis), University of Strathclyde, Glasgow, UK, 1998.
(20) Batterman, B. W. *Phys. Rev. Lett.* **1969**, *22*, 703.
(21) Golovchenko, J. A.; Batterman, B. W.; Brown, W. L. *Phys. Rev.* **1974**, *B10*, 4239.

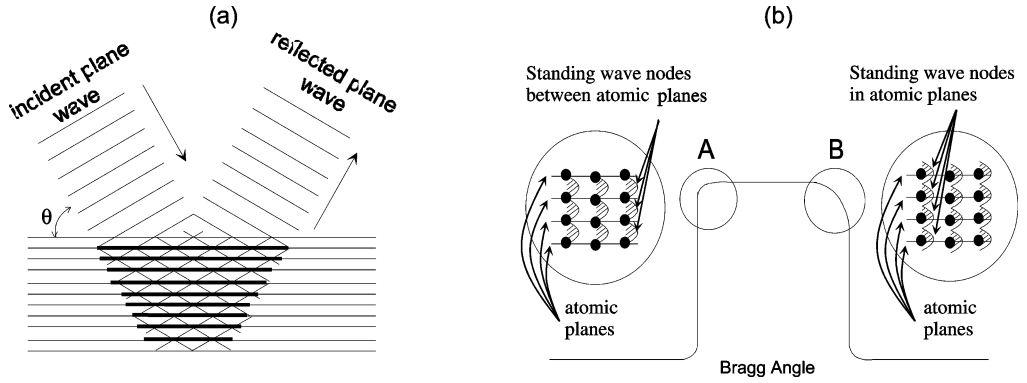

Figure 5. Schematic diagram illustrating the production and the movement of XSW resulting from dynamic X-ray diffraction in a nearly perfect single crystal: (a) XSW produced by interference between incident and diffracted beams; (b) schematic showing the movement of XSW nodes with respect to the atomic diffracting planes as a function of diffraction angle over the rocking curve range. The intensity deduction on the right-hand side of the rocking curve (inset B) compared to that of the left-hand side (inset A) reflects the X-ray absorption by the atoms of the host crystal material.

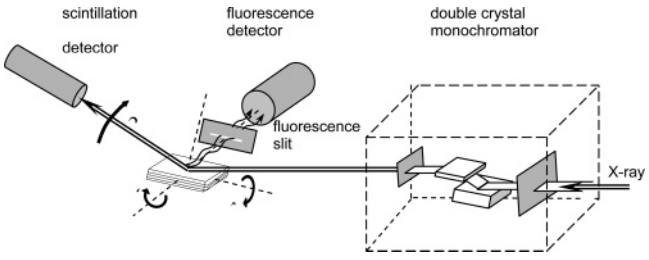

Figure 6. Setup for X-ray standing wave spectroscopy experiments on beamline X15A at NSLS, Brookhaven National Laboratory.

of incident beam (E_0), υ is the diffracted beam phase, and F^H and P^H are the coherent fraction and coherent position, respectively.

The XSW experiments were carried out on beamline X15A at the National Synchrotron Light Source (NSLS), Brookhaven National Laboratory, which was specially designed for high-resolution single-crystal XSW spectroscopy measurements.

In this, the alignment of Cr- and Mn-doped KDP single crystals was achieved using a high precision single crystal goniometer. The beamline was also equipped with a piezoelectric actuator providing an accurate movement of 0.25 arc/s for the detailed crystal rocking curve measurements. To determine the shape of the total fluorescence yield with respect to that of the associated Bragg peak, two detectors were simultaneously used. A NaI scintillation counter was used to record the shape of the rocking curve, while a single-element Ge solid-state detector linked to a multichannel analyzer was used to collect the fluorescence yield for the elements K, P, Mn, and Cr contained within the sample material over the rocking curve range (see Figure 6).

The XSW spectra for Cr- and Mn-doped KDP crystals were recorded using the 200 reflection with these planes being parallel to the sample surface. This experimental setup enabled the use of a fluorescence filter and therefore permitted simplification of the data analysis procedure involving the theoretical rocking curve and fluorescence yield curve fitting. Using available computer modeling procedures, the coherent position and the coherent fraction values were obtained (see theory and data analysis procedure[19,22]). In this, coherent position reflects the relative position of the absorbing atom between {200} planes and the coherent fraction reflects the associated atomic density.

2.4. Molecular Modeling. Geometric modeling of the lattice site revealed by XSW spectroscopy drawing upon the local atomic coordination indicated from the XAS measurements was effected via standard molecular modeling techniques. In this, the Cerius[2] program[23] together with the universal force field[24] was used to calculate the potential energy of the complex and the complex relative to the environment of the KDP crystal. Energy minimization was employed to optimize the conformation of the impurity complex itself and that of the impurity complex within the KDP crystal lattice environment. In this procedure, the potential energy of an arbitrary geometry was calculated as the sum of various two-body, three-body, and four-body interactions with the total potential energy being expressed as a sum of valence or bonded and nonbonded interactions. Iteration of the impurity site geometry within these constrainedly resulted in the final binding motif.

3. Results and Discussion

3.1. Crystal Growth. KDP crystals grown from the Cr-doped solutions displayed a dark green coloration while the crystals grown from the Mn-doped solutions were dark brown in coloration. Visual inspection revealed the impurities clearly segregated in the prismatic growth sectors of (100) and (010). All the doped crystals had a typical morphology elongated in the [001] direction with the prismatic {100} and {010} faces becoming tapered. However, at the lower solution pHs, the tapering angle was found to be larger and associated with a concomitant darker color within the effected crystal prismatic sectors, consistent with the enhancement of the habit modification effect for KDP at the lower pHs.

3.2. X-ray Absorption Spectroscopy. As crystals of Mn KDP were grown from a mixed solution of $MnCl_2$ and $KMnO_4$ in which Mn exists in a number of oxidation states, the oxidation state of the Mn within the KDP crystals was assessed by X-ray absorption near edge spectra (XANES). Figure 7 shows (XANES) spectra of the model compounds: Mn foil (Mn^0), $MnCl_2$ (Mn^{2+}), manganic acelylacetonate (Mn^{3+}), K_2MnO_3 (Mn^{4+}), and $KMnO_4$ (Mn^{7+}) together with the fluorescence XANES spectra of the Mn-doped KDP single crystal for comparison purposes. The data reveals that as the oxidation state of Mn increased, the pre-edge feature in the absorption spectrum became higher, with the absorption edge threshold shifting toward higher energies. A comparison of the spectra taken from the doped crystal with those taken from the other model compounds reveals both

(22) Cunningham, D. A. H.; Armstrong, D. R.; Clydesdale, G.; Roberts, K. J. *Faraday Discuss.* **1993**, *95*, 347.

(23) Cerius[2], Computational Instruments for Materials Research, Molecular Simulations International, Cambridge, UK.

(24) Rappe, A. K.; et al. *J. Am. Chem. Soc.* **1992**, *114*, (a) 10024 and (b) 10046.

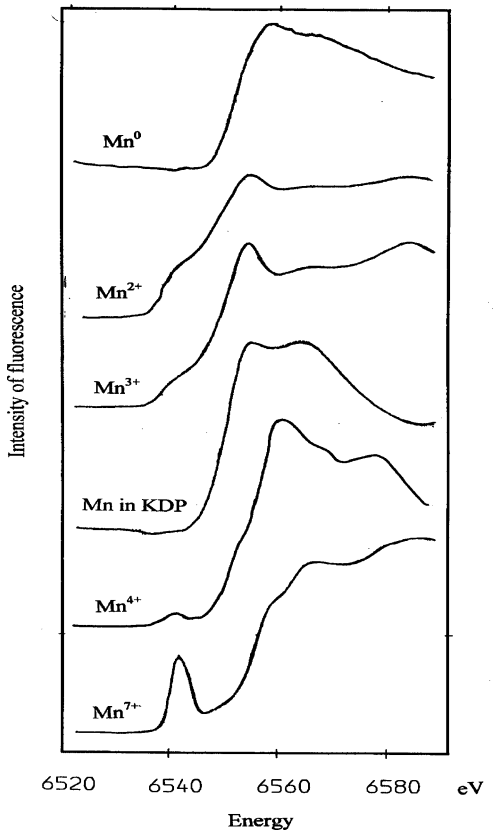

Figure 7. Fluorescence XANES spectra taken for the Mn-doped KDP crystal in comparison with transmission XANES spectra for representative model compounds involving several manganese valence states.

the edge position at 6555 eV and the near-edge feature at 6568 eV of Mn in KDP crystal to be close to that found for manganic acetylacetonate, i.e., manganese in its trivalent state.

Figure 8 shows the fit of the EXAFS and Fourier transform for Mn-doped KDP at the Mn K-edge for an incident angle of 15°. From the curve fitting, the likely backscattering atoms were identified together with the coordination numbers for the atoms and the associated central atom to nearest neighboring atom bond lengths, which are listed in Table 1 for the angles of 15°, 45°, and 75°.

The EXAFS analysis was consistent with three near neighboring shells of atoms surrounding the impurity atom of Mn within the KDP crystal lattice, O (1.87 Å), Cl (2.40 Å) and P (3.13 Å), which represent the averages of shell radii for the three different angles. The results from the similar analysis for Cr^{3+} in Cr-doped KDP crystals are given in Table 2.

For both Mn- and Cr-doped KDP, the EXAFS curve fitting for the first shell was found to be very precise, and the type and the coordinate number of the oxygen atom were determined with confidence. The oxygen positions in this shell are 1.87 and 1.903 Å distance from Mn and Cr, respectively.

For the second neighboring shells, the possible elements providing the better fitting were either chlorine or oxygen. Because oxygen was not likely to be at a distance between 2.3 and 2.5Å, it is probable that chlorine would form the second shell with the variation coordination number. This correlation would perhaps be due to some impurities being

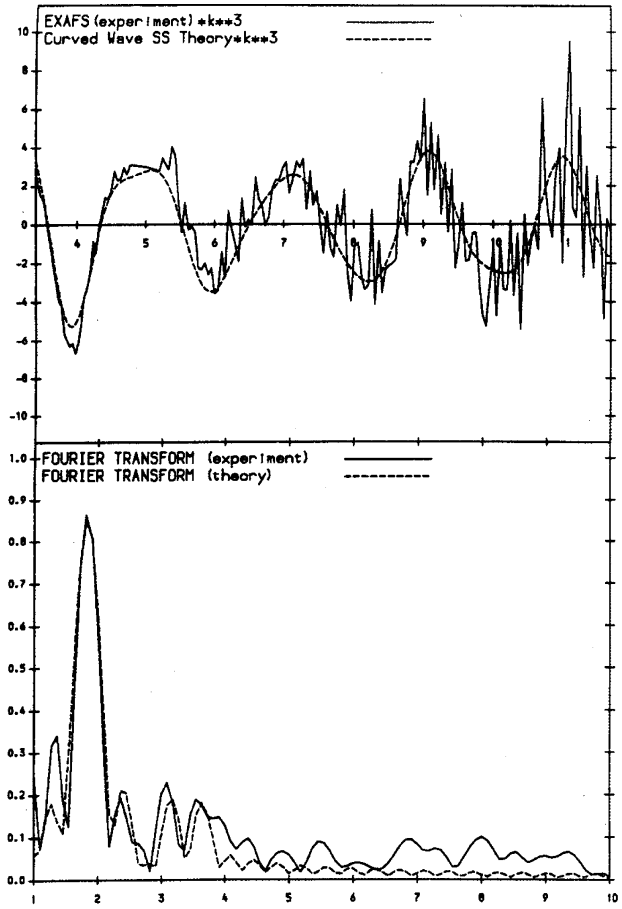

Figure 8. EXAFS and associated Fourier transform of Mn-doped KDP single crystal taken at the Mn K-edge at an incident angle of 15°.

Table 1. Summary of Results for the Curve Wave Fitting of the Mn K-edge EXAFS Spectra Taken of Mn^{3+}-Doped KDP Single Crystal at Incident Angles of 15°, 45°, and 75°, Showing the Atom Types, Coordination Numbers (*N*), Radius (*R*), and Debye Factors (σ^2) Associated with the Fitting

incidence angle (deg)	backscattering atom type	coordination number	radius (Å)	σ^2 (Å^2)
15	O	1.85	1.88	0.001
	Cl or O	0.2	2.35	0.001
	P or K	0.43	3.16	0.016
45	O	1.80	1.87	0.001
	Cl or O	0.33	2.43	0.009
	P or K	0.43	3.12	0.019
75	O	1.85	1.86	0.001
	Cl or O	0.35	2.44	0.009
	P or K	0.97	3.10	0.018

Table 2. Summary of Results for the Curve Wave Fitting of the Cr K-edge EXAFS Spectra Taken of Cr^{3+}-Doped KDP Single Crystal at Incident Angles of 15°, 45°, and 75°, Showing the Atom Types, Coordination Numbers (*N*), Radius (*R*), and Debye Factors (σ^2) Associated with the Fitting

incidence angle (deg)	backscattering atom type	coordination number	radius (Å)	σ^2 (Å^2)
15	O	3.6	1.903	0.001
	Cl or O	0.4	2.38	0.01
45	O	3.3	1.903	0.002
	Cl or O	0.7	2.35	0.007
75	O	3.0	1.910	0.002
	Cl or O	0.6	2.33	0.008

associated with one chlorine while others perhaps were associated with none.

EXAFS data indicated tentative evidence for a third shell correlation in Mn-doped KDP at 3.1 Å, although the type of

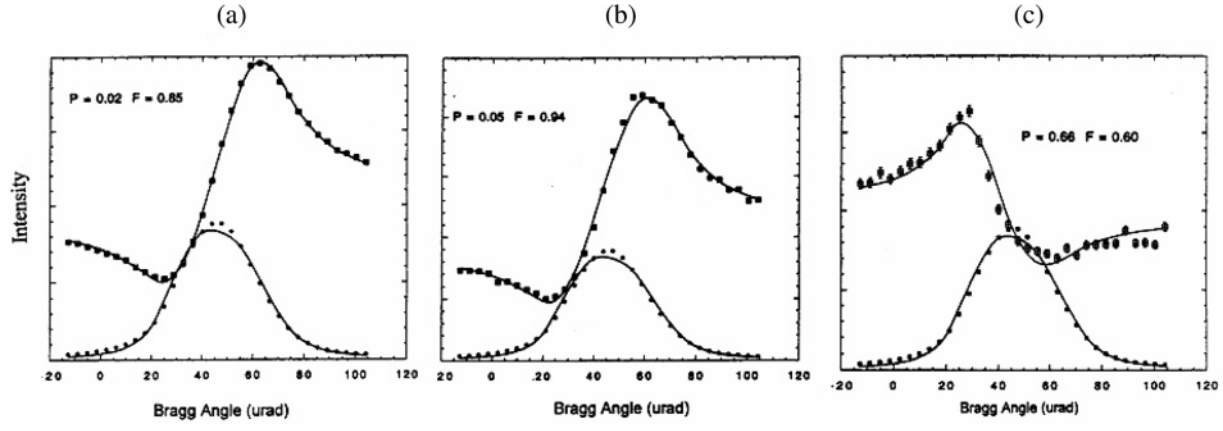

Figure 9. 200 reflection XSW spectra of Mn-doped KDP single crystals showing superimposition of the Bragg reflection rocking curve (lower) with the X-ray fluorescence intensity (upper). (a, left) K total fluorescence yield, (b, middle) P total fluorescence yield, and (c, right) Mn total fluorescence yield.

element could not be determined directly through the EXAFS curve fitting with any confidence. According to this radius distance, the element was likely to be of the host crystal material, such as phosphorus or potassium. The atomic number of the third shell of EXAFS at 75° for Mn-doped KDP was much bigger than those at 15° and 45°. Since the X-ray polarization was horizontal and perpendicular to the incident beam direction, the higher coordination number component of P or K at 75° of the [001] axis perhaps implies that the vector of Mn−P or Mn−K maintained a high angle with the [001] axis. The quality of the data of Cr-doped KDP was not sufficiently good enough to allow identification of the third neighboring shell around Cr.

3.3. X-ray Standing Wave Spectroscopy. X-ray standing wave analysis for KDP data, carried out by theoretically fitting the diffraction rocking curve profiles and the K, P, and Mn fluorescence yield spectra for the 200 reflection, are shown in parts a, b, and c of Figure 9, respectively, where the experimental data are simulated with the fitted patterns. The data reveals the fluorescence yield of Mn to display opposite profiles to that found in the P and K spectra. Mindful that the latter atoms are aligned on the {100} lattice planes, this clearly indicates that the Mn atomic site would be most likely consistent with an interstitial site within the KDP crystal lattice, which is also consistent with the result of a recent X-ray multiple diffraction study on KDP.[15] The coherent positions of Mn was determined to be 0.66 with respect to the KDP {200} atomic planes, whereas the coherent positions were, as expected, zero for the K and P, i.e., being located on the {200} plane surfaces.

The quantitative coherent position and fraction of Cr could not be determined from the Cr XSW spectra, due to the poor signal-to-noise ratio for the Cr fluorescence, reflecting high Cr content (stainless steel) in the XSW spectrometer apparatus. However, the fact that the overall shape of the Cr fluorescence yield XSW spectra was very similar to that of the Mn spectra clearly points to a similar interstitial site with a coherent position close to that found for Mn-doped KDP. The results of data analysis of 200 reflections for Mn- and Cr-doped KDP are summarized in Table 3.

Overall, these results contradicted the assumption that the trivalent impurities were incorporated within substitutional sites in the ADP/KDP crystal lattice, e.g. on the phosphate or the potassium sites as proposed by Cunningham et al.[2] and Byteva,[25] respectively. On the other hand, this work broadly supports the previous study by Barrett et al.,[1] i.e., that the impurity was at an interstitial site in the case of ADP, and that of Lai et al. for KDP.[14]

Table 3. Coherent Positions and Coherent Fractions of Mn, Cr, K, and P with Respect to {200} Atomic Planes of KDP Crystal

	Mn-doped KDP			Cr-doped KDP		
related to 200 planes	Mn	K	P	Cr	K	P
Coherent position, P^H	0.66	0	0	N/A[a]	0	0
Coherent fraction, F^H	0.60	0.85	0.94	N/A	0.02	0.02

[a] Similar to that of Mn.

3.4. Structural Modeling.

3.4.1. Solution Chemistry. In aqueous solution, the chemistry of transition metal ions, predominantly determined by the internal electron orbital structure with the nature of the ligands to which the ion can bind, is mostly influenced by the solution pH. This generates a substantial range of possible chemical compounds, each of which may exist in equilibrium with each other. For trivalent transition metals, octahedral complexes involving six equivalent ligands of water molecules are the most common,[26] since the electron orbitals of Cr^{3+} present octahedral symmetry with similar structures being expected for Mn^{3+} and Fe^{3+} complexes in solution. Thus, Cr^{3+} can be used as a representative example of these three species.

According to the studies of Matijevic et al.,[27] Cr complexes with phosphoric acid in the hydrolyzed species are particularly susceptible to occur. These complexes are expected to have various similar atomic configurations in solution. When $Cr(H_2O)_6^{3+}$ forms in a solution containing $H_2PO_4^-$, the likely mechanisms are as follows:

$$[Cr(H_2O)_6]^{3+} + H_2PO_4^- \rightarrow [CrH_2PO_4(H_2O)_5]^{2+} + H_2O \quad (2)$$

$$[CrH_2PO_4(H_2O)_5]^{2+} + H_2PO_4^- \rightarrow [Cr(H_2PO_4)_2(H_2O)_4]^+ + H_2O \quad (3a)$$

or

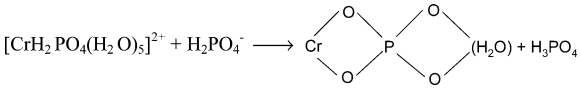

(3b)

Both steps 3a and 3b involve the loss of a water molecule from the chromium cation. Presumably step 3a would be favored, since the formation of a stable four-membered hydrated species would depend on the radius of the unhydrated metal ion. Other complexes can also be formed, depending on the concentration of $Cr(H_2O)_6^{3+}$ and the acidity of the solution.[28] The forms of the chromium complexes formed in the solution are thus as follows:

$$A = [H_2PO_4{-}Cr{-}H_2PO_4]^{+} \quad (4)$$

$$B = [H_2PO_4{-}Cr{-}HPO_4{-}Cr{-}H_2PO_4]^{2+} \quad (5)$$

$$C = [H_2PO_4{-}Cr{-}(HPO_4{-}Cr)_2{-}H_2PO_4]^{3+} \quad (6)$$

$$D = [H_2PO_4{-}Cr{-}(HPO_4{-}Cr)_3{-}H_2PO_4]^{4+} \quad (7)$$

$$E = [H_2PO_4{-}Cr{-}(HPO_4{-}Cr)_6{-}H_2PO_4]^{7+} \quad (8)$$

$$F = [H_2PO_4{-}Cr{-}HPO_4{-}Cr]^{4+} \quad (9)$$

$$G = [Cr{-}HPO_4{-}Cr]^{4+} \quad (10)$$

According to Redfern and Salmon,[29] all these complexes from A to G can exist in solution, and form A is likely to be the dominant form in solutions having a low concentration of Cr. As in the doped KDP crystal growth solution only a trace amount of the trivalent metal cations was added, it would thus be consistent that form A should be the likely dominant form. Mindful of this, this specific ionic complex was selected for further structural modeling. Such a model is attractive, since the phosphate groups in this complex could potentially mimic those on the KDP surfaces and hence perhaps easily adsorb at the crystal growth interface.

3.4.2. Modeling the Impurity Complex Structure. Accepting that the form A chromium−phosphate complex bound to four water molecules is predominantly produced in the solution, the complexed form $[H_2PO_4{-}Cr(H_2O)_4{-}H_2PO_4]^{+}$ highlights the comparison of the atomic configuration of this ionic complex with that of the surface structure of the KDP crystal. This should be considered in the light of previous studies by Buckley and Whetstone[30,31] who attempted to provide a model for impurity adsorption at crystal growth interface despite the lack of any detailed atomic structural information about impurity.

Considering the adsorption of atomic species during the growth of pure KDP, crystals, which remain neutral in charge, can absorb a molecular cluster built of KH_2PO_4 subunits. If a cluster of two phosphate groups bound together through a hydrogen bond were to be adsorbed on the crystal surface, it would be in the form of a $[H_2PO_4{-}H{-}O_4PH]^{2-}$ complex followed by the two K^+ cations needed to maintain the system charge balance. However, when a chromium impurity complex $[H_2PO_4{-}Cr(H_2O)_4{-}O_4PH]$, in which $Cr(H_2O)_4^{3+}$ has displaced the proton between the two associated phosphates, approaches the crystal surface, it may be trapped on the surface, providing that the steric conformation of the two phosphate ions in the adsorbed complex is similar to that of the two-phosphate cluster expected for the pure KDP growth case. Because the adsorption of this single complex has already provided a neutral charge to the crystal, the two associated K^+ cations would be likely to be repelled in order to maintain the system change balance. Due to its atomic size, the success or not of the chromium complex adsorption would be thus dependent on the separation distance of the two phosphate ligands for which there are two possible configurations, i.e., phosphate ions in either trans- and cis-configurations.

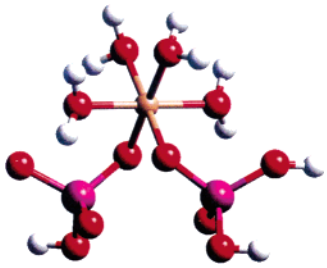

Figure 10. The proposed conformation of the neutral cis-configured impurity complex $[H_2PO_4{-}Cr(H_2O)_4{-}O_4PH]$ as optimized by molecular modeling.

The conformation of the Cr complex was constructed in Cerius[2] and optimized using the Minimizer molecular modeling tool. Reflecting upon the fact that a 4.4 Å separation distance between the phosphates for the trans-configured complex would be too large compared to the 3.7 Å separation distance on the {100} crystal face, this complex was excluded for further consideration. The cis-configured complex, however, has a phosphate separation distance on the order of 3.8 Å (see Figure 10), therefore providing a more viable structure for surface adsorption onto the KDP {100} surfaces and occupying the positions of two adjacent surface phosphate groups as shown in Figure 11.

According to de Vries,[16] the prismatic{100} face has both positive K^+ ion and negative $H_2PO_4^-$ groups. Therefore, the neural charged impurity complex $[H_2PO_4{-}Cr(H_2O)_4{-}O_4PH]$ can be easily adsorbed on the prismatic faces of KDP. However, reflecting upon the positive charge on the pyramidal {101} faces, i.e., due to the fact that the surfaces only contain K^+ ions, the neutral complex may experience the difficulty in binding onto these habit faces for subsequent adsorption. This model hence provides an attractive rationalization for the observed sector-specific segregation of trivalent impurity in ADP/KDP.

3.4.3. Modeling of Impurity Species within Bulk Crystal Lattice. The proposed model of the impurity complex adsorbed at the {100} crystal surface revealed that the $[H_2PO_4{-}Cr(H_2O)_4{-}O_4PH]$ complex has the potential to displace the bulk ionic cluster $[H_2PO_4{-}H{-}O_4PH]^{2-}$ and hence, in principle, can be incorporated during KDP crystal growth. Alternatively, this complex could also be described as a $Cr(H_2O)_4^{3+}$ group being substituted for one hydrogen in the bulk structure with the Cr atom occupying the hydrogen site. Clearly, due to the size difference between these two species, the space at the H^+ site would not be sufficient to

(25) Byteva, I. M. *J. Cryst. Growth* **1968**, *58*, 26.
(26) Greenwood, N. N.; Earnshaw, A. *Chemistry of the Elements*; Pergamon Press: Elmsford, NY, 1984.
(27) Matijevic, E.; Lindsay, A. D.; Kratohril, S.; Jones, M. F.; Larson, R. I.; Cayey, N. W. *J. Colloid Interface Sci.* **1971**, *36*, 273.
(28) Holroyd; Salmon, J. E. *J. Chem. Soc.* **1956**, 269.
(29) Redfern, J. P.; Salmon, J. E. *J. Chem. Soc.* **1961**, 291.
(30) Buckley, H. E. *Zeit. Kristallogr.* **1934**, *88*, 248 and 381.
(31) Whetstone, J. *Discuss Faraday Soc.* **1954**, *5*, 132.

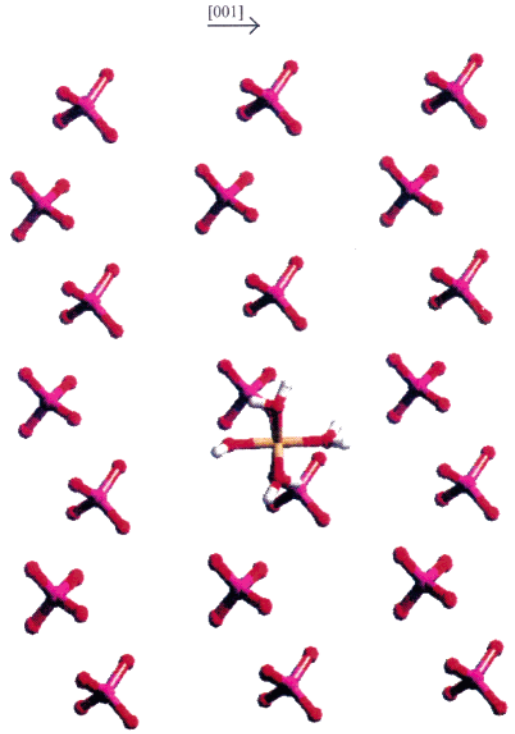

Figure 11. Molecular packing diagram on the {100} crystal surface showing the location of a cis-configured neutral impurity complex as adsorbed onto the prismatic habit face of KDP.

accommodate a large species such as $Cr(H_2O)_4^{3+}$. Therefore, this complex species would have to occupy some of the space occupied by other ionic groups, via the creation of vacancy defect site. As hydrogen has a charge of +1 and $Cr(H_2O)_4^{3+}$ has a charge of +3, to maintain an ionic charge balance, the incorporation of $Cr(H_2O)_4^{3+}$ by the KDP lattice would be expected to be associated with the removal of one or more cation groups with a total charge of +2. Although an incorporation of one or more anion groups with a total charge of −2 might be an alternative way to maintain the system charge balance, the removal of cation groups would be favorable in this respect because of the need of space for the excessive size of the incorporated impurity complex species.

Mindful of the above, the removal of cations was modeled using the structure visualization tool within Cerius[2]. In this, using bulk KDP crystallographic structure, a hydrogen between a pair of phosphates on the same {100} lattice plane was removed. The $Cr(H_2O)_4^{3+}$ species was substituted with the Cr centered at the original H-atom position, the bonds between Cr and the two PO_4 groups in the KDP structure being established. The lengths of all the six bonds of Cr−O (four to H_2O molecules and two to PO_4 groups) were set to 1.93 Å, in agreement with the EXAFS experimental result, by translating the $Cr(H_2O)_4^{3+}$ complex along the [100] direction and also by rotating it around the axis connecting two bonded oxygens in order to locate free space within the crystal lattice. During this operation the symmetry of Cr with respect to the two linked phosphates was maintained, i.e., with the distances between the Cr and its two associated P atoms being kept the same. Within this constraint, there was only one viable lattice site for the complex, which was also consistent with that proposed in the surface model. For example, inclination of the complex either toward the [001] or [001] directions by rotation brought the water molecules of the complex too close to the oxygen atoms in the other phosphate groups, hence requiring further removal of oxygens or even phosphate groups providing structures that were clearly not rational.

At the optimized position, the distances between the atoms in the complex and the atoms of the host crystal were measured. It was found that the closest distance from the two water molecules of the complex with respect to the two K^+ ions was only 0.6 Å, and hence, these two K ions were removed not only to create a space for the complex but also to satisfy the charge balance requirements for the system, as predicted in the surface model, e.g.

$$Cr(H_2O)_4^{3+} \rightarrow 2V_K^{+} + V_H^{+} \qquad (11)$$

It should be noted that the above analysis is consistent with that of the surface model prediction. All distances between the complex atoms and neighboring atoms of the host crystal were beyond 2.5 Å. The structural model for the complex in bulk crystal lattice summarized in Figure 12a,b shows the [010] projection view of the structural model of pure crystal and impurity-incorporated crystal, while Figure 12c shows the associated [001] projection. The bulk model only showed the structure of an impurity complex incorporated through the specific [100] face, which is associated with one of four symmetry-related orientations for the complex incorporated through the {100}, {100}, {010}, and {010} faces.

3.4.4. Rationalization of the Structural Model with the Experimental Measurements. The EXAFS analysis showed an increase of the atomic number in the third shell at 75° polarization. The impurity model in the crystal also indicated that the vector of Cr−P was close to the direction perpendicular to the [001] axis at the distance of about 3.1 Å. On this basis, the atom in the third shell found from the fitting of the EXAFS spectra would be consistent with a phosphorus ion site.

Taking the bond length of the impurity metal atom to oxygen from the first shell analysis of EXAFS spectra, Mn^{3+} and Cr^{3+} were placed in the modeled positions within the KDP crystal lattice. The relative positions of the metal ions with respect to {200} atomic planes and their distances to the phosphorus atoms of the host material were measured within Cerius[2] and are given in Table 4. The table reveals the structural model of the complex in KDP to be in excellent agreement with the experimental results provided by the combination of XSW and EXAFS analysis.

The structure of an idealized impurity complex having an octahedral conformation thus has been built up on the basis of the knowledge of the electron orbital structure of the transition metal ions: in this case, cation bonded to four water molecules within the KDP crystal lattice. However, EXAFS analysis showed that this may not be completely true as the coordination number of 1.85 in the first shell at all the incident angles for the Mn-doped KDP is much smaller than that for the Cr-doped KDP. This could imply that Mn might be bonded to a smaller number of water

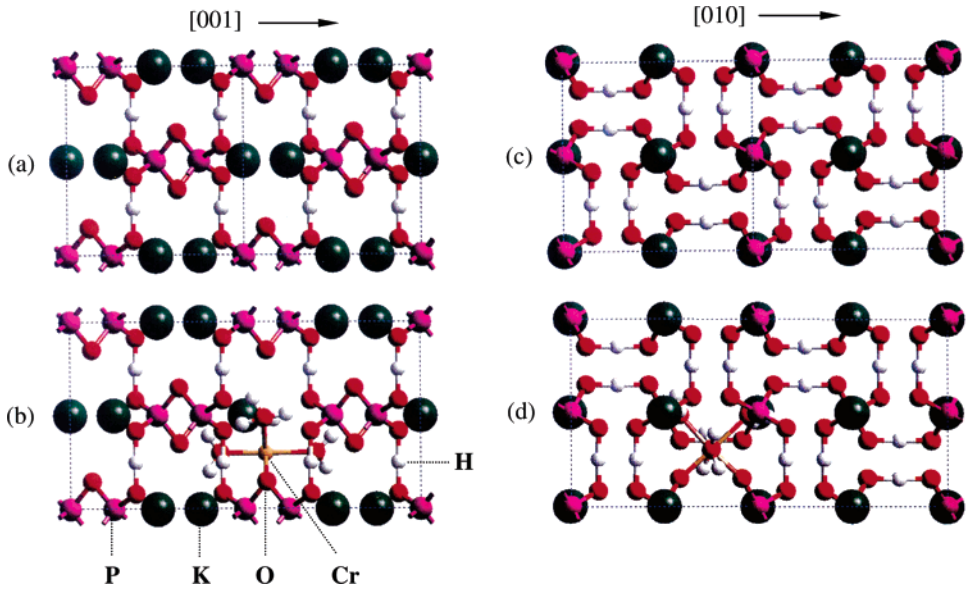

Figure 12. Molecular packing diagrams illustrating the proposed lattice structure for Cr impurity as incorporated into KDP single crystal. (a) [010] projection of pure crystal lattice; (b) [010] projection of impurity-doped crystal lattice; (c) [001] projection of pure crystal lattice; (d) [001] projection of impurity-doped crystal lattice.

Table 4. Modeled and Experimental Results of the Relative Positions of Mn and Cr with Respect to the {200} Crystal Lattice Plane in KDP and M−P Distances, respectively (M = Mn^{3+} or Cr^{3+})

	Mn−O = 1.87 Å (EXAFS result)	Cr−O = 1.903 Å (EXAFS result)
modeling relative position for {200} plane	0.67	0.68
XSW relative position for the {200} plane	0.66	~0.66
modeling distance of MsP	3.21 Å	3.25 Å
EXAFS distance of MsP	3.12 Å	

molecules besides the two bonds to the oxygen atoms in the phosphate groups in KDP, and the water molecules could be in random positions with the electronic bonding orbitals not being fully saturated.

4. Conclusions

Molecular and 3-D structural modeling studies on the incorporation of trivalent transition metal ions into the KDP crystal lattice have allowed an impurity structure model for the incorporation to be built up. The analysis is consistent with the incorporation of the impurity as a hydrated complex adsorbed onto the crystal {100} faces, reflecting the structural similarity of the phosphate groups in the impurity complex to those in the crystal surface atomic arrangement. The impurity in the KDP crystal is found to occupy an interstitial site associated with creation of one hydrogen atom with two potassium ionic vacancies as needed both to maintain charge balance and to allow for steric considerations. The structural model is supported by the analysis of both XAS and XSW experimental data. With the knowledge of the structural nature of the trivalent metal complexes adsorbed in KDP crystal, it should now be possible to examine the detailed interface kinetic mechanism for the crystal habit modification of this material on the molecular scale.

Acknowledgment. We are grateful for the CCLRC Daresbury and Brookhaven National Laboratory, respectively, for the provision of experimental beamtime at the SRS and NSLS. This work was initiated as a part of Ph.D. study of one of the authors (Xiaojun Lai), supported by the ORS scheme and the Department of Pure and Applied Chemistry at the University of Strathclyde in Glasgow, UK. The synchrotron radiation experiments at the NSLS were supported by EPSRC grant (GR/K/80518).

CM0478881